Development of a dual transformation method and its application to electronic and nuclear dynamics in intense laser fields

Hirohiko Kono, Isao Kawata, and Yuichi Fujimura
Department of Chemistry, Graduate School of Science, Tohoku University

A dual transformation technique that can deal with awkward Coulomb potentials is developed for electronic wave packet dynamics. The technique consists of the variable transformation of the Hamiltonian and the transformation of the wave function with a normalization constraint. The time evolution is carried out by the alternating-direction implicit method. The operation of the transformed Hamiltonian on the wave function is implemented by using five-point finite difference formulas. We apply it to H atom and a realistic 3D model of H_2^+. Efficient time evolution schemes are provided by imposing the variable transformations on the following requirements: the transformed wave function is zero and analytic at the nuclei; the equal spacings in the scaled coordinates correspond to grid spacings in the unscaled coordinates that are small near the nuclei (to cope with relatively high momentum components near the nuclei) and are large at larger distances. The validity of the transformations is also enforced by the fact that the missing volume in phase space decreases with decreasing spacings.

1. Introduction

Femtosecond technology has opened up a new field of study as to nonlinear optical processes such as above-threshold ionization and high-order harmonic generation of emission. The intensity can be so high to induce tunneling ionization. In the high-intensity and low-frequency range, the Coulomb potential distorted by the laser electric field forms a "quasi-static" barrier through which an electron can tunnel. High-order harmonics are generated when the ejected electron circles back to the vicinity of the nucleus (rescattering).[1] Electronic dynamics in intense fields involves such large amplitude motions.

For molecules, nuclear motion is also involved in the dynamics of the system. Recent experiments and theories in a strong laser field case ($> 10^{11}\,\mathrm{W/cm^2}$) have underscored the combined process of photodissociation and photoionization. It has been experimentally revealed that the kinetic energies of fragments are consistent with Coulomb explosions at specific internuclear distances in the range of 7–10 a.u.[2,3] An explanation for this finding is as follows: ionization rates at the critical internuclear distances exceed those near the equilibrium internuclear distance and those of dissociative fragments, and ionization to higher-charge states occurs when the nuclei pass through the critical range. The fact that ionization is enhanced at critical internuclear distances suggests that strong correlation between the electronic motion and the nuclear configuration/motion exists in intense laser fields.

Although various numerical methods for electronic dynamics in laser fields have been proposed, it is not an easy task to simulate, *e.g.*, large amplitude motions of an electronic wave packet. There exist two kinds of approach. One is the expansion using spatially delocalized bases.[4] In this approach, the time-dependent wave function is expanded in terms of state-specific states, *i.e.*, bound, autoionizing, and scattering states of the field-free Hamiltonian. The grid representation is complementary to the state-specific expansion. For electronic dynamics, however, one must cope with the awkward Coulomb potential characterized by its long range and its singularity at the origin. Because of those difficulties, the performance of the conventional grid methods is very poor for Coulomb systems.

Recently, we have been developing an efficient grid method to simulate electronic dynamics accurately.[5] The choice of coordinate systems is crucial. In Ref. 5, the following three requirements are imposed on the coordinate system to be employed: (1) the wave function is transformed so that it is zero at the Coulomb singular point (which ensures that the numerical difficulties concerning the singularity are avoided); (2) the differential operators can be well evaluated by the finite difference method even near the Coulomb singular points; (3) the equal spacings in the new (scaled) coordinates correspond to grid spacings in the cylindrical coordinates that are small near the nuclei (to cope with relatively high momentum components near the nuclei) and are large at larger distances therefrom. The transformed Schrödinger equation is integrated in time by the alternating-direction implicit method (ADI).[6] We have applied the method to H. The cylindrical coordinate ρ for the electron is transformed as $\rho = \xi^{3/2}$, where ξ is a scaled coordinate. We have also succeeded in including nuclear motion for a realistic 3D model of H_2^+.[7] Although the nuclear motion is restricted to the polarization direction z of the laser electric field (perpendicular to ρ), the electron moves in three dimensional space. The two electronic coordinates z and ρ and the internuclear distance R are treated quantum mechanically without using the Born-Oppenheimer approximation.

In this paper, we generalize the dual transformation technique, *i.e.*, the method of consistently transforming both of the wave function and the Hamiltonian for wave packet dynamics. The transformation of ρ is expressed as $\rho = f(\xi)$, where the function is chosen to satisfy the three requirements (1)–(3) described above. Scaling is extended to the unscaled z coordinate as $z = g(\zeta)$. Various functions of the transformations are examined in different ranges of grid spacings $\Delta\xi$ and $\Delta\zeta$, by comparing the wave packet calculated by the

dual transformation technique with the exact one.

2. Method

2.1 Dual transformation

In this work, we apply the dual transformation technique to H and the 3D model of H_2^+ employed in Ref. 8. In the model, the following assumptions are made: the electric field of the applied laser is linearly polarized along the z-axis; the nuclear motion is restricted to the polarization direction. Because of the cylindrical symmetry, the z-component of the electronic angular momentum, $m\hbar$, is conserved; the electronic degrees of freedom to be considered are two cylindrical coordinates z and ρ.

The center-of-mass motion of this three-body system can be separated from internal coordinates. The Hamiltonian for the internal motions is written as (throughout this paper atomic units are used)

$$H = -\frac{1}{m_p}\frac{\partial^2}{\partial R^2} - \frac{1}{2\mu}\left(\frac{\partial^2}{\partial\rho^2} + \frac{1}{\rho}\frac{\partial}{\partial\rho} + \frac{\partial^2}{\partial z^2}\right) + \frac{m^2}{2\rho^2} + \frac{1}{R} + V(\rho, z, R) + V_\varepsilon(z, t), \tag{1}$$

where R is the internuclear distance, m_e and m_p are electron and nuclear masses, and

$$\mu = \frac{2m_p m_e}{2m_p + m_e}. \tag{2}$$

The potential $V(\rho, z, R)$ is the sum of the Coulomb interactions

$$V(\rho, z, R) = -\frac{1}{\sqrt{\rho^2 + (z - R/2)^2}} - \frac{1}{\sqrt{\rho^2 + (z + R/2)^2}}, \tag{3}$$

and $V_\varepsilon(z, t)$ is the dipole interaction between the molecule and the electric field $\varepsilon|(t)$ of a laser pulse

$$V_\varepsilon(z, t) = z\mathcal{E}(t). \tag{4}$$

Here, ρ and z are measured with respect to the center of mass of the two nuclei. For the H atom, the R-degree of freedom is eliminated from Eq. (1), and Eq. (3) is replaced with $-1/\sqrt{\rho^2 + z^2}$(μ is the reduced mass of H).

We would like to spatially discretize the Hamiltonian to solve the time-dependent Schrödinger equation

$$i\frac{\partial}{\partial t}\Phi(\rho, z, R) = H\Phi(\rho, z, R). \tag{5}$$

We use the finite difference method to evaluate the differential operators contained in the Hamiltonian. For the cylindrical coordinate system, however, the finite difference method does not give sufficient accuracy. We propose here the scaled cylindrical coordinate system as

$$\rho = f(\xi), \quad z = g(\zeta), \tag{6}$$

where f and g are functions of scaled coordinates ξ and ζ.

In addition to the variable transformation of the Hamiltonian, we have to transform the wave function to avoid the numerical difficulties concerning the Coulomb singularity. The original wave function $\Phi(\rho, z, R)$ which is in general finite at the nuclei must be transformed to a function $\Psi(\xi, \zeta, R)$ that is zero at the nuclei. This demand on the transformed wave function, *i.e.*, the requirement (1) in Section 1, must be satisfied under a normalization condition. The original wave function $\Phi(\rho, z, R)$ is normalized as

$$\int_0^\infty dR \int_0^\infty d\rho \int_{-\infty}^\infty dz\rho|\Phi(\rho, z, R)|^2 = 1. \tag{7}$$

When the finite difference method is used, it is generally difficult to conserve the norm of the wave function. It has been known[5] that to make stable and accurate the time evolution scheme based on the finite difference method the following normalization condition should be imposed on the transformed wave function $\Psi(\xi, \zeta, R)$

$$\int_0^\infty dR \int_0^\infty d\xi \int_{-\infty}^\infty d\zeta|\Psi(\xi, \zeta, R)|^2 = 1. \tag{8}$$

Note that the volume element for normalization is $dRd\xi d\zeta$ not like $\xi dRd\xi d\zeta$.

The transformed wave function that satisfies the normalization condition Eq. (8) is uniquely determined as

$$\Psi(\xi, \zeta, R) = \sqrt{f(\xi)f'(\xi)g'(\zeta)}\Phi(f(\xi), g(\zeta), R), \tag{9}$$

where a function with a prime denotes the derivative with respect to its argument. Inserting Eq. (9) into Eq. (5), one obtains the following Schrödinger equation:

$$i\frac{\partial}{\partial t}\Psi(\xi, \zeta, R) = \hat{H}\Psi(\xi, \zeta, R), \tag{10}$$

where the transformed Hamiltonian $\hat{H}$ is given by

$$\hat{H} = K_R + K_\xi + K_\zeta + \frac{m^2}{2\rho^2} + V + V_\varepsilon. \tag{11}$$

The kinetic energy parts with respect to coordinates ξ, ζ, and, R, *i.e.*, K_ξ, K_ζ, and K_R are expressed as

$$K_\xi = T_\xi + \frac{1}{4\mu f'^4(\xi)}\left[\frac{7}{2}f''^2(\xi) - f'(\xi)f'''(\xi)\right] - \frac{1}{8\mu f^2(\xi)}, \tag{12a}$$

$$K_\zeta = T_\zeta + \frac{1}{4\mu g'^4(\zeta)}\left[\frac{7}{2}g''^2(\zeta) - g'(\zeta)g'''(\zeta)\right], \tag{12b}$$

$$K_R = -\frac{1}{m_p}\frac{\partial^2}{\partial R^2}, \tag{12c}$$

where

$$T_\xi = -\frac{1}{4\mu}\left[\frac{1}{f'^2(\xi)}\frac{\partial^2}{\partial\xi^2} - \frac{\partial^2}{\partial\xi^2}\frac{1}{f'^2(\xi)}\right], \tag{13a}$$

$$T_\zeta = -\frac{1}{4\mu}\left[\frac{1}{g'^2(\zeta)}\frac{\partial^2}{\partial\zeta^2} - \frac{\partial^2}{\partial\zeta^2}\frac{1}{g'^2(\zeta)}\right]. \tag{13b}$$

2.2 Time evolution

The formal solution of Eq. (10) is expressed as

$$\Psi(t_{n+1}) = \exp[-i\Delta\hat{H}(t_{n+1/2})]\Psi(t_n) + O(\Delta t^3), \tag{14}$$

where $\Phi(t_n)$ is the wave function at time $t_n = n\Delta t + t_0$ and $\hat{T}$ is the time ordering operator. The Hamiltonian in the second version of Eq. (14) is that at the midpoint of the time step, $t_{n+1/2} = t_n + \Delta t/2$. If the time step Δt is sufficiently small, the propagator $\exp[-i\Delta\hat{H}(t_{n+1/2})]$ can be replaced with an approximate propagator that is accurate up to a certain order of Δt. It has been known that the alternating-direction implicit method (ADI) provides short time propagators of which quality is characterized by the second-order accuracy in time and the stability for various potentials.[6] In addition to these points, as will be demonstrated, the ADI is amenable to variable transformations. Let us assume that $\hat{H}(t_{n+1/2})$ is decomposed into three operators $A(t_{n+1/2})$, $B(t_{n+1/2})$, and $C(t_{n+1/2})$. According to the ADI, the time evolution operator $\exp[-i(A+B+C)\Delta t]$ is expressed as

$$e^{-i(A+B+C)\Delta t} = \frac{1}{1+iA\Delta t/2}\frac{1}{1+iB\Delta t/2}\frac{1-iC\Delta t/2}{1+iC\Delta t/2} \times (1-iB\Delta t/2)(1-iC\Delta t/2) + O(\Delta t^3). \quad (15)$$

The actual operation on the wave function is separated into three steps by introducing artificial intermediate states $\Psi^{n+1/3}$ and $\Psi^{n+2/3}$

$$(1+iC\Delta t/2)\Psi^{n+1/3} = (1-iC\Delta t/2)(1-iB\Delta t/2) \times (1-iA\Delta t/2)\Psi(t_n), \quad (16a)$$

$$(1+iB\Delta t/2)\Psi^{n+2/3} = \Psi^{n+1/3}, \quad (16b)$$

$$(1+iA\Delta t/2)\Psi(t_{n+1}) = \Psi^{n+2/3}, \quad (16c)$$

which is known as the Dyakonov scheme. The wave function $\Psi(t_{n+1})$ can be obtained by solving Eqs. (16) in order. As shown below, the dynamics of the electronic and nuclear wave packet can be pursued without invoking any approximations.

When the differential operators involved in A, B, and C are chosen to be those of different degrees of freedom, Eqs. (16) can be reduced to three sets of one-dimensional implicit problems by using the finite difference method with appropriate boundary conditions. For H_2^+, the three operators K_ζ, K_ξ, and K_R in the Hamiltonian Eq. (11) must be confined in A, B, and C separately. For instance, Eq. (16a) is then reduced to a set of systems of simultaneous linear algebraic equations for the unknown $\Psi^{n+1/3}$: Eqs. (16) can be reduced to three sets of systems of simultaneous equations. The systems of equations are pentadiagonal for the five-point finite difference scheme, which can be solved efficiently by using LU decomposition.

2.3 Explicit forms for variable transformation

We are now in a position to explicitly determine f and g functions of scaled coordinates ξ and ζ. To fulfill the three requirements (1)–(3) in Section 1, we choose the following forms

$$f(\xi) = \xi\left(\frac{\xi^n}{\xi^n+\alpha^n}\right)^\nu, \quad (17a)$$

$$g(\zeta) = [1-(1-\beta)\exp(-\zeta^2/\gamma^2)]\zeta, \quad (17b)$$

where the parameters α and γ are widths of ρ- and z-ranges where the potential V is relatively deep, and β is the parameter to shorten ζ-grid spacings near z=0. Around the singular points (located along $\xi = 0$), the prefactor $\sqrt{ff'g'}$ changes as $\approx \sqrt{(1+n\nu)\beta}\xi^{(2n\nu+1)/2}/\alpha^{n\nu}$. The requirement (2) that the transformed wave function must be analytic, demands that the order of the power of ξ, $(2n\nu+1)/2$, must be a natural number. The number $n\nu$ must be chosen out of half odd numbers. Then, the transformed wave function given by Eq. (9) is zero at the nuclei; the requirement (1) is automatically fulfilled.

Inverting equally spaced points in ξ and ζ onto ρ and z, one finds that the grid spacings in ρ and z are proportional to f' and g', respectively. As ξ increases, f' changes from $(1+n\nu)(\xi/\alpha)^{n\nu}$ to 1; as ζ increases, g' changes from β to 1. When $\beta < 1$ and $\alpha >> \Delta\xi$, the requirement (3) is met. Then, grid spacings along rho- and z-directions decrease as approaching to the singular points. When the cylindrical coordinate system ($\alpha = 0$ and $\beta = 1$) is employed, the split operator time evolution technique together with the use of FFT is applicable to the transformed Hamltonian (because the prefactors of the differentials in the transformed Hamiltonian are independent of the coordinates), but the efficiency as a numerical method is very low. Poor performance of the cylindrical coordinate system originates from the fact that the requirements (2) and (3) are not satisfied. For the cylindrical coordinate system, the transformed wave function is not analytic around the nuclei because $\sqrt{ff'g'} \approx \sqrt{\rho}$. The Fourier series expansion of the transformed wave function converges very slowly.

In Eq. (13a), the symmetrized product form of $\partial^2/\partial\xi^2$ and $1/f'^2(\xi)$ is adopted as well as in Eq. (13b). If symmetric difference formulas are applicable to T_ξ, the grid representation of the symmetrized product form is symmetric: the grid representation of K_ξ is then still hermitian. The norm is hence strictly conserved (without numerical roundoff errors). However, the finite difference representation of

$$\frac{\partial^2}{\partial\xi^2}\frac{\Psi(\xi,\zeta,R)}{f'^2(\xi)}, \quad (18)$$

at the point $\xi = \Delta\xi$ next to the line $\xi = 0$ requires evaluating $\Psi(\xi,\zeta,R)/f'^2(\xi)$ at $\xi = 0$, which is generally nonzero. It is not allowed to simply put the boundary condition $\Psi(\xi = 0, \zeta, R) = 0$ into the element. To avoid this difficulty in the actual numerical scheme, we use an asymmetric form

$$K_\xi = -\frac{1}{2\mu f'^2(\xi)}\left[\frac{\partial^2}{\partial\xi^2} - \frac{2f''(\xi)}{f'(\xi)}\frac{\partial}{\partial\xi}\right] - \frac{1}{4\mu f'^4(\xi)}\left[\frac{5}{2}f''^2(\xi) - f'(\xi)f'''(\xi)\right] - \frac{1}{8\mu f^2(\xi)}. \quad (19)$$

This form is still hermitian, but the finite difference representation is only approximately symmetric except when f is a linear function of ξ (cylindrical coordinate ρ). We will show that the loss of population due to the asymmetry is negligible when the transformation functions f and g are chosen properly.

3. Results and discussion

3.1 Application to H

We first apply our method to the time evolution of a hydrogen atom in the case where no laser field is turned on and the atom is initially (at $t = 0$) in the ground state $1s$. We designate the field-free transformed Hamiltonian as $\hat{H}_0$. It should be pointed out that the time evolution of $1s$ is the worst case in applying the present method. As the average of the radial coordinate becomes larger, the steep fall of the Coulomb potential around the nucleus damages the accuracy less severely. Since only two variables ξ and ζ are involved, we use the Peaceman-Rachford method which is a two-dimensional version of the ADI method. The time evolution for Δt is then separated into two steps: $(1 + iB\Delta t/2)\Psi^{n+1/2} = (1 - iA\Delta t/2)\Psi(t_n)$ and $(1 + iA\Delta t/2)\Psi(t_{n+1}) = (1 - iB\Delta t/2)\Psi^{n+1/2}$.

We demonstrate how much the norm and overlap of the $1s$ state calculated by our method decrease or change with time. The norm and overlap are defined as $\langle\Psi^f_{1s}(t)|\Psi^f_{1s}(t)\rangle$ and $\langle\Psi^f_{1s}(0)|\Psi^f_{1s}(t)\rangle$, respectively, where $\Psi^f_{1s}(0)$ is the discretized wave function whose amplitudes at the grid points are identical with the analytic $1s$ transformed wave function $\Psi_{1s} = \sqrt{2ff'g'}\exp(-\sqrt{f^2+g^2})$, and $\Psi^f_{1s}(t)$ denotes the time evolution of $\Psi^f_{1s}(0)$ for the discretized form of the field-free transformed Hamiltonian, $\hat{H}'_0$. The integrals with respect to ξ and ζ are performed by using the trapezoidal rule.

It should be noted that $\Psi^f_{1s}(0)$ is not identical with the ground state of the discretized Hamiltonian, $\hat{H}'_0$, $\Psi'_{1s}(0)$. The initial wave function $\Psi^f_{1s}(0)$ includes excited state components $\{\Psi'_{2s}, \Psi'_{3s}, \dots\}$ of $\hat{H}'_0$, *i.e.*, $\Psi^f_{1s}(0) = \sum c_j(0)\Psi'_j$, where j runs from $1s$ (c_{1s} is dominant). As the discretized form is better approximated to the Hamiltonian (11), the norm and overlap at $t = 0$ are closer to unity and the difference between Ψ'_{1s} and $\Psi^f_{1s}(0)$ becomes smaller ($c_{1s} \sim 1$). The time evolution of Ψ^f_{1s} calculated by our method is expressed as

$$\Psi^f_{1s}(t) = \sum_j c_j(t)\Psi'_j\exp(-itE'_j) \tag{20}$$

where E'_j are eigenvalues of $\hat{H}'_0$ and $c_j(t)$ are expected to be slowly varying functions of time. The norm and overlap change with time as $\langle\Psi^f_{1s}(t)|\Psi^f_{1s}(t)\rangle = \sum|c_j(t)|^2$ and $\langle\Psi^f_{1s}(0)|\Psi^f_{1s}(t)\rangle = \sum c^*_j(0)c_j(t)\exp(-itE'_j)$, respectively. If the time evolution scheme generates no errors, the coefficients $c_j(t)$ are time-independent, *i.e.*, $c_j(t) = c_j(0)$. The time-dependence of $c_j(t)$ originates from the inaccuracy of the time evolution scheme.

We test transformations by changing n and ν in Eq. (17a). As shown in Section 2.3, near $\xi = 0$, the transformed wave function changes as $\propto \xi^{(2n\nu+1)/2}$. Since we apply the finite difference method, the transformed wave function must change linearly or quadratically with ξ: $n\nu$ must be $1/2$ or $3/2$. In what follows, we numerically test two cases for $n\nu = 1/2$ and the $n = 1$ and $\nu = 3/2$ case.

The $n = 1$ and $\nu = 1/2$ transformation

Shown in Fig. 1 are norms and overlaps for the five-point finite difference scheme. The norms are denoted by solid lines and the absolute values of overlaps are denoted by lines with open circles. Two cases of different grid spacings are compared: Case (a) $\Delta\xi = \Delta\zeta = 0.26$ (red); Case (b) $\Delta\xi = \Delta\zeta = 0.13$ (green). The grid boundaries are chosen as $\xi_{max} = 65.0$ (the grid end in ρ is 54.3) and $\zeta_{max} = 55$ (the corresponding grid ends in z are ± 52.9). For Case (a), $N_\xi = 250$ and $N_zeta = 423$. The time step used to evolve the wave function is $\Delta t = 0.05$ throughout this paper. As shown in Fig. 1, $\sqrt{\langle\Psi^f_{1s}(t)|\Psi^f_{1s}(t)\rangle} \approx |\langle\Psi^f_{1s}(0)|\Psi^f_{1s}(t)\rangle|$. This means that $c_{1s}(t) \approx 1$ and $c_j(t) \approx 0$ for $j \neq 1s$. The generation of excited states of $\hat{H}'_0$ is negligible as well as the leakage in norm. Except in the early stage where the norm decreases, $c_{1s}(t)$ is nearly time-independent (although it oscillates).

The ground state for $\hat{H}'_0$, Ψ'_{1s}, is obtained by operating an energy filter on $\Psi^f_{1s}(0)$ and eliminating the excited components. The norm $\langle\Psi'_{1s}(t)|\Psi'_{1s}(t)\rangle$ and the overlap $|\langle\Psi'_{1s}(0)|\Psi'_{1s}(t)\rangle|$ do not change up to 6 or 7 digits. This again proves that the coefficients $c_j(t)$ in Eq. (20) are nearly time-independent, *i.e.*, $c_j(t) = c_j(0)$. The source of phase errors arising in the time evolution of the wave function is therefore only the inaccuracy of eigenvalues of the discretized Hamiltonian $\hat{H}'_0$. The eigenvalues of $\hat{H}'_0$ are highly accurate; the ground state energy is -0.49943 for Case (a) and -0.49971 for Case (b). The virial theorem is also fulfilled to very high accuracy; for the ground state of $\hat{H}'_0$, the ratio of the potential energy to the kinetic energy is -1.9974 for Case (a) and -1.9998 for Case (b).

The solutions of the five-point scheme converge to that of the Schrödinger equation by reducing $\Delta\xi$, $\Delta\zeta$ and Δt; that is, the scheme is consistent with the Schrödinger equation. For the parameters chosen in Fig. 1, the error does not grow exponentially with time. Practically, the method of the $n = 1$ and $\nu = 1/2$ transformation is unconditionally stable. For the cylindrical coordinate system, the accuracy is hardly improved by using higher order finite differences nor by using smaller spacings. For Case (a), the absolute value of the overlap is 0.88 for the five-point scheme; for Case (b) the values go up by 0.02–0.03.

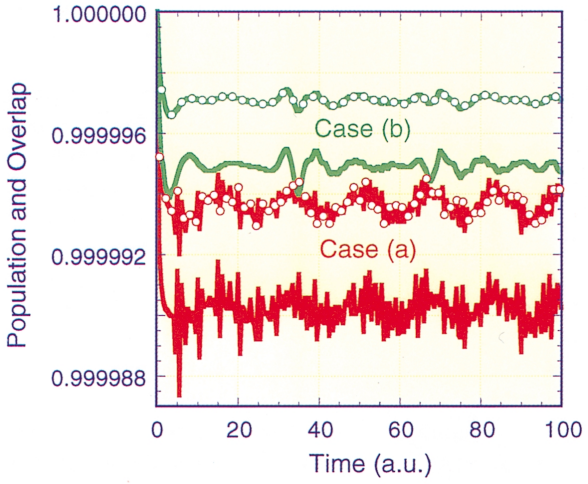

Fig. 1. Norms and overlaps of the $1s$ state calculated by the five-point finite difference scheme for $n = 1$ and $\nu = 1/2$. The two cases (a) and (b) for different grid spacings are compared. See the text. The norms are denoted by solid lines and the absolute values of overlaps are denoted by lines with open circles. The parameters for variable transformations are as follows: $\alpha = 28.3$, $\beta = 0.2$ and $\gamma = 32$.

The $n = 1$ and $\nu = 3/2$ transformation

Comparing numerical results, we find that the accuracy is a little worse for the $n = 1$ and $\nu = 3/2$ transformation than for the $n = 1$ and $\nu = 1/2$ one. While the $1s$ transformed wave function for $n\nu = 1/2$ increases linearly with ξ around the nucleus, it increases quadratically for $n\nu = 3/2$. For both cases, the initial norm at $t = 0$ is accurate up to 7 or 8 digits. The difference in accuracy comes from the fact that the asymmetry of the finite difference representation of Eq. (19) on grid points $\xi_j = j\Delta\xi$ is severer for the present transformation than for the $n = 1$ and $\nu = 1/2$ transformation.

The $n = 1/2$ and $\nu = 1$ transformation

Among those we have tested, the $n = 1$ and $\nu = 1/2$ transformation provides most accurate results when $\Delta\xi$ is as small as in Case (a). For low bound states, the accuracy is improved by increasing α. Extremely large α, however, should not be used when higher excited/continuum states are involved in the dynamics of the wave packet because the grid spacing in ρ space increases as $\Delta\rho \propto f' \approx (1 + n\nu)(\xi/\alpha)^{n\nu}$ until ξ reaches α . In the range where the potential is nearly flat, the grid spacing $\Delta\rho$ must be constant. For Eq. (18a), f' becomes constant where $\xi > \alpha$. Different transformations of Eq. (18a) should be compared for a fixed α.

When computational ability is limited or large grids are required to propagate the wave packet, we recommend to use another transformation of $n\nu = 1/2$, *i.e.*, the $n = 1/2$ and $\nu = 1$ case. When the grid spacings are much larger than in Case (a), say, $N_\xi = 60$ and $N_\zeta = 100$ (the other parameters are the same as before), the $n = 1/2$ and $\nu = 1$ transformation is superior to the $n = 1$ and $\nu = 1/2$ one. For large spacings, while the accuracy of the finite difference method in evaluating the differentials is nearly the same for both transformations, the asymmetry in the finite difference representation near $\xi = 0$ is much smaller for the $n = 1/2$ and $\nu = 1$ transformation than for the $n = 1$ and $\nu = 1/2$ one.

3.2 Classical phase space analysis

As shown in this paper, variable transformation together with the consistent transformation of the wave function is indispensable for the wave packet dynamics in Coulomb systems. In the following, using the phase space analysis, we examine why the efficincy of the grid representation is enhanced by the variable transformations tested in Section 3.1. In general, wave packets decay exponentially in classically forbidden regions of phase space. The representation efficiency can therefore be optimized by minimizing the missing phase space, *i.e.*, the classically allowed phase space that cannot be covered by the grid representation or by minimizing the wasted phase space area relative to the phase space covered by the grid representation (Fattal et al.[9]) have applied the method to the H_2^+ eigenvalue problem). The maximum momentum with ξ in the grid representation is given by $\pi/\Delta\xi$. The function $f(\xi)$ should be chosen so that the phase space between $-\pi/\Delta\xi$ and $\pi/\Delta\xi$ covers the classically allowed phase space as well as possible. Here we do not give the details of the analysis. To conclude, with decreasing $\Delta\xi$, the missing volume approaches zero for the $n\nu$=1/2 and $n\nu$=3/2 transformations, while it diverges in a logarithmic way for the cylindrical coordinate system.[10]

3.3 3D packet simulation of H_2^+

The two transformations of $n\nu = 1/2$ are also tested for the 3D H_2^+. The dissociative process is taken as the example. To that end, first, the exact ground state (of the vibrational quantum number $v = 0$ in $1\sigma_g$) of the 3D full system is prepared by operating an energy filter on an approximate ground state to eliminate the excited components. Next, the molecule is excited by a weak ultrashort pump pulse from the ground state onto 1su. The frequency used is $\omega = 0.43$ (105 nm) which corresponds to the energy gap between $1\sigma_g$ and $1\sigma_u$ at the equilibrium internuclear distance $R = 2.0$ and the pulse duration is $T = 100$ (2.5 fs). The pump field is put into the dipole interaction Eq. (4). A perturbative iteration scheme59 with respect to the dipole interaction is used to simulate the excitation process of the 3D packet in the weak field limit. To perform the time evolution of the packet required in the scheme, we solve the transformed Schrödinger Eq. (10) by using the ADI method. At the end of the pump process ($t = 0$), the electronically excited component of the packet (the first order component with respect to the dipole interaction) is normalized to unity. After $t = 0$, the dissociative motion is pursued; the excited component is propagated without an external field.

To illustrate the packet dynamics, we integrate the 3D packet

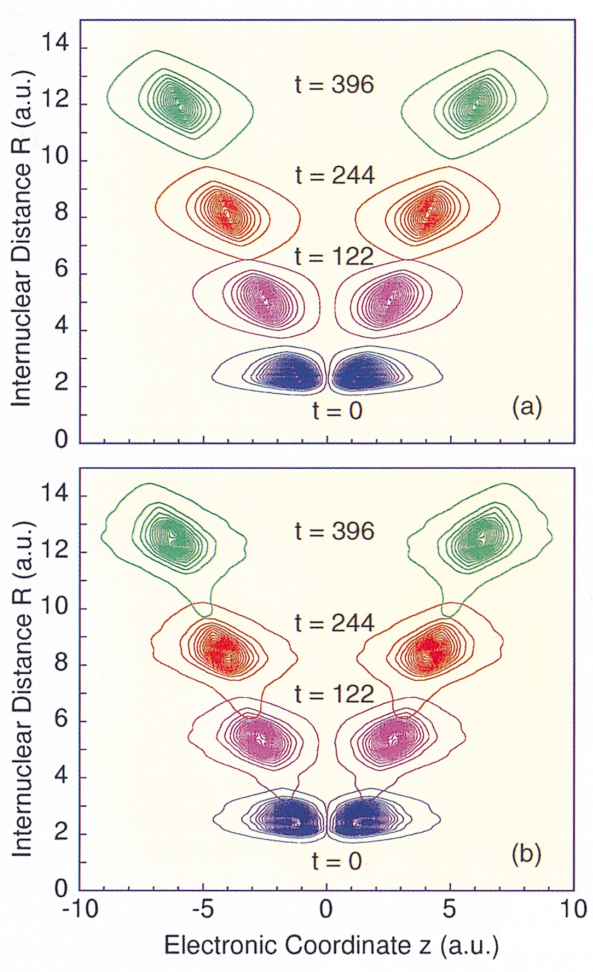

Fig. 2. Contour maps of the time-dependent probability $\int |\Phi(\rho, z, R)|^2 \rho d\rho$. A sequence of snapshots shows that the packet pumped on $1\sigma_u$ moves toward larger internuclear distance. The

origin $t = 0$ in time is the end of the pump pulse. In (a), $n = 1$ and $\nu = 1/2$; $N_\xi = 151$ and $N_\zeta = 207$. In (b), the $n = 1/2$ and $\nu = 1$ transformation; $N_\xi = 19$ and $N_\zeta = 57$.

over ρ . Snapshots of the probability obtained by integrating the 3D packet with respect to ρ are shown in Fig. 2. The grid ends are chosen as $\rho_{max} = 8.83$ and $z_{max} = 10$. We choose $\alpha = 28.3$ and $\Delta R = 0.05$. In Fig. 2(a), $n = 1$ and $\nu = 1/2$. The numbers of grid points are enough large, although no transformation is used for z-coordinate; $N_\xi = 151$ and $N_\zeta = 207$ ($\Delta\xi = 0.1$, $\Delta\zeta = 0.1$). The excitation and dissociation dynamics in Fig. 2(a) is regarded as the exact one. As known from the existence of the nodal line at $z = 0$, the packet prepared by the pump pulse is electronically $1\sigma_u$. The errors in electronic phases attached to the wave function are small enough to simulate the excitation process; the vibrational phases are also accurate enough to simulate dissociation process. In Fig. 2(b), the $n = 1/2$ and $\nu = 1$ transformation is used. The numbers of grid points are reduced to $N_\xi = 19$ and $N_\zeta = 57$. The main features of the dynamics are well simulated even with the parameter set used in Fig. 2(b), except that the wave packet trails the skirt of low density and the relative nuclear velocity is a little larger than the exact one.

3.4 H_2^+ in intense fields

We have investigated effects of the nuclear motion on enhanced ionization and on electron transfer between the two nuclei.[7)] Correlations between the electronic and nuclear motions are extracted from the full dynamical calculation.

4. Summary and conclusions

We established the dual transformation technique for wave packet dynamics. The technique contains both the variable transformation of the Hamiltonian and the transformation of the wave function with a normalization constraint. We applied it to Coulomb systems, *i.e.*, the H atom and the 3D model of H_2^+. When the variable transformation functions and the grid spacings are properly chosen in the dual transformation, the virial theorem is fulfilled to very high accuracy. For the dual transformation, the singularity is removed without violating the Schrödinger equation and any variational procedure is unnecessary.

In this paper, the wave functions are expressed in cylindrical coordinates. The dual transformation technique is in principle applicable to any coordinate systems. The procedure in solving a given problem is to choose the best coordinate system for describing the dynamics and then to apply the dual transformation. In conclusion, the dual transformation is a solid technique that provides efficient time evolution schemes for Coulomb systems. The accuracy and stability reach the level usually required for wave packet dynamics.

This work was supported in part by the Department of High-Density Optical Pulse Generation and Advanced Material Control Techniques.

References

1) P. B. Corkum: Phys. Rev. Lett. **71**, 1994 (1993).
2) P. A. Hatherly, M. Stankiewicz, K. Codling, L. J. Frasinski, and G. M. Cross: J. Phys. B **27**, 2993 (1994).
3) S. Chelkowski and A. D. Bandrauk: J. Phys. B **28**, L723 (1995); T. D. G. Walsh, F. A. Ilkov, S. L. Chin, F. Châteauneuf, T. T. Nguen-Dang, S. Chelkowski, A. D. Bandrauk, and O. Atabek: Phys. Rev. A **58**, 3922 (1998).
4) S. Dionissopoulou, Th. Mercouris, A. Lyras, and C. A. Nicolaides: Phys. Rev. A **55**, 4397 (1997).
5) H. Kono, A. Kita, Y. Ohtsuki, and Y. Fujimura: J. Comput. Phys. **130**, 148 (1997).
6) A. R. Mitchell: Computational Methods in Partial Differential Equations, (Wiley, New York, 1969).
7) I. Kawata, H. Kono, and Y. Fujimura: Chem. Phys. Lett. **289**, 546 (1998); J. Chem. Phys. **110**, 11152 (1999).
8) S. Chelkowski, T. Zuo, O. Atabek, and A. D. Bandrauk: Phys. Rev. A **52**, 2977 (1995).
9) E. Fattal, R. Baer, R. Kosloff, and D. Kosloff: Phys. Rev. E **53**, 1217 (1996).
10) I. Kawata and H. Kono: J. Chem. Phys. **111**, 9498 (1999).